Applied Mathematics and Computation 421 (2022) 126907

Contents lists available at ScienceDirect

Applied Mathematics and Computation

journal homepage: www.elsevier.com/locate/amc

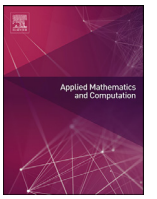

Closed form parametrisation of 3D clothoids by arclength with both linear varying curvature and torsion

Marco Frego

Faculty of Science and Technology, Free University of Bolzano, Bolzano, Italy

A R T I C L E I N F O

Article history:
Received 31 August 2020
Revised 23 December 2021
Accepted 28 December 2021
Available online 22 January 2022

Keywords:
Clothoid
Euler spiral
3D curve
Magnus expansion
Commutator-Free

A B S T R A C T

The extension from the planar case to three dimensions of the clothoid curve (Euler spiral) is herein presented, that is, a curve parametrised by arc length, whose curvature and torsion are linear (affine) functions of the arc length. The problem is modelled as a linear time variant system and its stability is studied with Lyapunov techniques. Closed form solutions in terms of the standard Fresnel integrals are for the first time presented and they are valid for a wide family of clothoids; for the remaining cases, numerical methods of order four, based on Lie algebra, Magnus Expansions and Commutator-Free Expansions are provided. These geometric integrators have been optimised to be easily implemented with few lines of code and require only matrix-vector products (avoiding explicit matrix exponentials at each iteration). The achieved computational efficiency has a dramatic impact for several real-time applications, especially for designing trajectories for flying vehicles, as previous approaches were fully numeric and could not take advantage of the present closed form solutions, which render the computation of the 3D clothoid as computationally expensive as its planar companion.

1. Introduction

In this work, the extension to three dimensions of the clothoid curve is presented. A clothoid is a planar curve whose curvature is a linear (affine) function of the arclength and was studied for the first time by Euler and Bernoulli [1–5]. It is a transcendent curve, which can be expressed in closed form by means of Fresnel integrals [6,7]. Relying on special functions, the clothoid is computationally more expensive to evaluate and manipulate than other classic curves used in the applications [8,9], such as lines and arcs, biarcs, polynomials and splines, rational functions and NURBS. Nevertheless, the clothoid is being recognised as one of the most suitable primitive curves in a series of applications [2], as it turns out to be the natural solution of a variety of problems in the applied sciences. It is also appreciated for its appealing shape in design applications [10], and is referred to as a *fair curve*. The key features are the simple (and yet effective) expression of its curvature and the natural parametrisation by arc length, which makes it superior as compared to the family of (rational) polynomial curves showing irrational curvatures, torsions and lengths [2,7].

The planar clothoid has been thoroughly investigated by several researchers that can be divided into two main categories: the first one applies clothoids for engineering purposes [11–16]; the second one focuses on providing algorithms and methods for the former [3,4,17–20]; both list of references are far from being complete. The present paper belongs to the latter category. The most relevant results established in literature have been provided by the control community, the

E-mail address: marco.frego@unibz.it

https://doi.org/10.1016/j.amc.2021.126907
0096-3003/

applied mathematics and computer graphics fields. Known results include theoretical aspects [21]: the evaluation of the curve, the interpolation with various degrees of continuity [6,22], extension to splines of clothoids [4,23], the intersection of curves [24], and more specifically in control theory, optimisation of smooth speed profiles [5,25] and distance from a nominal path [26,27]. Most of these contributions and the results of the present work are collected in an open-source C++ library with Matlab interface [28,29].

In the field of mechatronic and control engineering, clothoids are popular as motion primitives for path planning, since they naturally model the trajectory of a car-like vehicle moving at constant speed [5,30] and they may also extend the Markov-Dubins curves [31,32]. An important feature related to the linear varying curvature is that the adoption of a clothoid requires to linearly actuate the steering wheel, which is related to the lateral accelerations experienced by the mechatronic system and therefore to the overall comfort [33,34].

The extension to three dimensions is important to take advantage of these properties also in flying vehicles, such as drones, helicopters, UAV, [35,36]. The advantage is to allow linear movements with respect to the horizontal plane, thus reducing undesired vertical forces. Other applications in science and engineering, other than the historic ones like road and railway design since the first works of Markov, are the modelling of human locomotion [37,38], of blood vessels [39], or rat whiskers [40], the design of rollercoaster [41,42]; in this latter case, the forces acting on passengers are maximised, rather than minimised.

The useful clothoid's properties have been extended to three dimensions only by means of fully numeric approaches. The aim of the present study is to illustrate the cases when an explicit and efficient closed form solution is available, as well as a geometric numeric integrator for the remaining cases.

The paper has the following structure, firstly the fundamental problem of this extension process is discussed, i.e., the definition of a 3D clothoid, as the planar case does not generalise to higher dimensions in a straightforward (and universally accepted) manner. To this end, the mathematical background is introduced in Section 2.1, together with the collocation of the paper in the state-of-the-art (Section 2.2). Section 3 formalises the problem of the 3D clothoid and studies some of its properties. The solution to the general problem in Lie Groups is presented in Section 4 together with an efficient numerical method based on the Magnus Expansion. Two particular cases of great interest for generality and computational efficiency (closed form solutions) are developed in Section 5. Section 6 provides numerical tests that validate the accuracy and efficiency of the presented methods. Finally, in Section 7, the conclusions are drawn and future research directions proposed.

2. Background and literature

2.1. Parametric space curves: the Frenet-Serret frame

The first problem faced is how to extend the clothoid from the planar to the spatial case. In particular, the torsion of the curve must be determined. In the accepted definition of torsion as the *second* curvature, and in sight of the fundamental theorem of space curves, the most natural extension in 3D is to assume the torsion linear (affine) with the arc length.

Theorem 1 (Fund. thm. of space curves, [43])**.** *Given two differentiable functions $\kappa(s) > 0$ and $\tau(s)$, for $s \in I$, there exists a regular parametrised curve $\gamma : I \mapsto \mathbb{R}^3$ such that s is the arc length, $\kappa(s)$ is the curvature and $\tau(s)$ is the torsion of γ. Any other curve $\hat{\gamma}$ that satisfies the same conditions differs from γ by a linear map φ of $\mathbb{R}^3$ with positive determinant and by a constant vector $\boldsymbol{c} \in \mathbb{R}^3$ such that $\hat{\gamma} = \varphi \circ \gamma + \boldsymbol{c}$, or in other words, by a rigid motion.*

Therefore, as the curvature and torsion completely define a curve, it seems only natural to extend the request of linearity also to the torsion. Before discussing other extensions provided in literature, we recall some definitions and properties of the geometry of space curves in order to compare the present and the other possible approaches. Velocity and acceleration are associated to a parametric spatial curve $\gamma : I = [t_0, t_1] \subset \mathbb{R} \mapsto \mathbb{R}^3$ given by $\gamma(t) = (x(t), y(t), z(t))$, where the parameter t is not necessarily the arc length: $\boldsymbol{v}(t) = \dot{\gamma}(t)$, $\boldsymbol{a}(t) = \dot{\boldsymbol{v}}(t) = \ddot{\gamma}(t)$. Related to the curve γ are also its speed and arclength:

$$\dot{s}(t) = ||\boldsymbol{v}(t)|| \quad \text{and} \quad s(t) = \int_{t_0}^{t} \dot{s}(\xi)\, \mathrm{d}\xi\,. \tag{1}$$

The widely known Frenet-Serret frame is defined by the unit tangent vector $\boldsymbol{t}$, the normal vector $\boldsymbol{n}$ and the binormal vector $\boldsymbol{b}$, the classic formulas for a general parametrisation of γ are:

$$\boldsymbol{t}(t) := \frac{\dot{\gamma}(t)}{||\dot{\gamma}(t)||}, \qquad \boldsymbol{n}(t) := \boldsymbol{b}(t) \wedge \boldsymbol{t}(t), \qquad \boldsymbol{b}(t) := \frac{\dot{\gamma}(t) \wedge \ddot{\gamma}(t)}{||\dot{\gamma}(t) \wedge \ddot{\gamma}(t)||}.$$

Taking the derivatives of the previous expressions yields the definition of two important quantities, the curvature κ and the torsion τ of the curve. They are written concisely as:

$$\begin{bmatrix} \dot{\boldsymbol{t}}(t) \\ \dot{\boldsymbol{n}}(t) \\ \dot{\boldsymbol{b}}(t) \end{bmatrix} = ||\dot{\gamma}(t)|| \cdot \left(\begin{bmatrix} 0 & \kappa(t) & 0 \\ -\kappa(t) & 0 & \tau(t) \\ 0 & -\tau(t) & 0 \end{bmatrix} \otimes \boldsymbol{I}_3 \right) \cdot \begin{bmatrix} \boldsymbol{t}(t) \\ \boldsymbol{n}(t) \\ \boldsymbol{b}(t) \end{bmatrix},$$

where $\boldsymbol{I}_3$ is the identity matrix, $\otimes$ is the Kronecker product, that ensures the resulting matrix is 9×9.

Remark 2. For brevity's sake, many books of differential geometry neglect the Kronecker product. When the context is non ambiguous, this notation is followed.

Explicitly, the curvature and the torsion are:

$$\kappa(t) = \frac{||\dot{\gamma}(t) \wedge \ddot{\gamma}(t)||}{||\dot{\gamma}(t)||^3}, \qquad \tau(t) = \frac{(\dot{\gamma}(t) \wedge \ddot{\gamma}(t)) \cdot \dddot{\gamma}(t))}{||\dot{\gamma}(t) \wedge \ddot{\gamma}(t)||^2}.$$

In view of the natural parametrisation of the curve with $t = s(t)$, i.e. by its arclength, the previous general expressions reduce to simpler relations. Starting from the arc length parametrisation (1), being the curve regular, it is possible to solve for $t = t(s)$: from $s(t) \equiv s(t(s))$ it follows that $\dot{s}(t) = \dot{s}(t)||\dot{s}(t)||$ and thus $||\dot{s}(t)|| = ||\dot{\gamma}(t)|| = 1$ has unitary norm and the curve has unit speed everywhere. The Frenet-Serret frame takes the simpler form

$$\boldsymbol{t}(s) := \gamma'(s), \qquad \boldsymbol{n}(s) := \frac{\boldsymbol{t}'(s)}{||\boldsymbol{t}'(s)||} = \frac{\gamma''(s)}{||\gamma''(s)||}, \qquad \boldsymbol{b}(s) := \boldsymbol{t}(s) \wedge \boldsymbol{n}(s) = \frac{\gamma'(s) \wedge \gamma''(s)}{||\gamma'(s) \wedge \gamma''(s)||}.$$

Similarly to the general parameter case, the relation for the derivatives of the frame simplifies to

$$\begin{bmatrix} \boldsymbol{t}'(s) \\ \boldsymbol{n}'(s) \\ \boldsymbol{b}'(s) \end{bmatrix} = \begin{bmatrix} 0 & \kappa(s) & 0 \\ -\kappa(s) & 0 & \tau(s) \\ 0 & -\tau(s) & 0 \end{bmatrix} \begin{bmatrix} \boldsymbol{t}(s) \\ \boldsymbol{n}(s) \\ \boldsymbol{b}(s) \end{bmatrix}, \tag{2}$$

so that the curvature and the torsion become

$$\kappa(s) = ||\gamma''(s)||, \quad \tau(t) = \frac{(\gamma'(s) \wedge \gamma''(s)) \cdot \gamma'''(s)}{||\gamma'(s) \wedge \gamma''(s)||^2},$$

or, more compactly, $\kappa(s) = ||\boldsymbol{t}'||$ and $\tau(s) = -\boldsymbol{b}' \cdot \boldsymbol{n}$.

2.2. Literature and comparisons

The choice of linear (affine) torsion is not the only possibility to extend to space a planar clothoid. The first paper that covers the extension to the 3D space of clothoids dates back to 2001 in [42], the torsion is not considered and the extension is done by iteratively refining a control polygon to match both the arc-length parametrisation as well as a linear distribution of the binormal vector.

About ten years later, in [44], with a similar approach, the supporting plane of a planar clothoid is rigidly tilted to match the final point in the 3D space. Despite being simple and intuitive, this approach loses the arclength parametrisation as well as the linearity of the curvature and of the torsion.

In the same years, [45–48] propose a numerical scheme based on variational principles to extend the clothoid to space, which is based on the gradient descent method to minimise the energy of the 3D curve. The clothoid is shown to be the solution of this optimisation problem. The proof of several properties of the space clothoid is also presented, including invariance to similarity transformation like translation, rotation and scaling; symmetry, i.e., the curve that connects the point $\boldsymbol{p}_0$ to $\boldsymbol{p}_1$ with initial and final tangents $\boldsymbol{t}_0$ and $\boldsymbol{t}_1$ is the same as the curve that joins $\boldsymbol{p}_1$ to $\boldsymbol{p}_0$ with initial and final tangents $-\boldsymbol{t}_1$ and $-\boldsymbol{t}_0$; extensibility; smoothness and roundness. All these properties render the clothoid a *fair curve*, acknowledged to be eye-pleasing and therefore suitable for artistic purpose. In fact, the Authors employ it for archaeological reconstruction of ancient sculptures and objects, such as the curly hair in broken head sculptures or for the ridges of Hellenistic lamps. Their focus is more on the geometric properties of the curve rather than to the development of a high performance numerical algorithm. Indeed the computational issues of this minimisation are in the convergence and the low order (one) of the gradient descent method.

In 2013, [49] presented the concept of super space clothoids in computer graphics with application to dynamic hair modelling. Although they recognise the Lie group structure of the problem, they do not attempt an analytic solution of it, stating that, in general, the problem cannot be solved formally. In the present study it is shown how for a wide combination of curvatures and torsions, a closed form solution exists in terms of the standard Fresnel integrals, hence a 3D clothoid is not essentially computationally heavier than a standard planar spiral arc. We also give precise conditions on when this is possible in terms of an easy test on the parameters of curvature and torsion. In [49], a numeric solution of the problem based on a non trivial power series is given, which takes into account the numerical difficulties of this stiff problem as numerical cancellation. Since the differential Eq. (2) evolves on a rotation group (this topic is discussed in the next sections), a polynomial expansion is not the best solution because, in general, the result does not belong to this group. They solve this issue by a rather involved subdivision method inspired by multiple precision arithmetics. When the closed form is not possible, we rely, instead, on a Lie group geometric integrator, that by construction evolves on the Lie group and preserves the orthonormality of the tangent, normal and binormal vectors. For details on numerical methods on Lie groups the reader is addressed to [50–52] and their references.

Finally, there is a completely different way of extending the clothoid, using the so-called intrinsic spline, introduced for planar curves in [53]. This formulation of the problem is very elegant, and the explicit curve equation can be written as:

$$x(s) = \int_0^s \cos\vartheta(\xi)\sin\varphi(\xi)\,\mathrm{d}\xi, \qquad y(s) = \int_0^s \sin\vartheta(\xi)\sin\varphi(\xi)\,\mathrm{d}\xi, \qquad z(s) = \int_0^s \cos\varphi(\xi)\,\mathrm{d}\xi, \tag{3}$$

where $\vartheta(\xi)$ and $\varphi(\xi)$ are polynomials. These are the integrals of the spherical coordinates, thus the arc-length parametrisation and orthonormality of the frame naturally arise. The curvature and torsion, however, are not linear, apart from the planar case, where the intrinsic spline reduces to the clothoid if ϑ is the usual quadratic polynomial. In the general case, dropping the dependence of s, we have

$$\kappa(s) = \sqrt{\varphi'^2 + \vartheta'^2(1-\cos^2\varphi)}, \qquad \tau(s) = \frac{\vartheta'(\vartheta'^2\sin^2\varphi + 2\varphi'^2)\cos\varphi - (\vartheta'\varphi'' - \vartheta''\varphi')\sin\varphi}{\varphi'^2 + \vartheta'^2\sin^2\varphi}.$$

Another important issue is that the integrals appearing in (3) are highly oscillatory and their practical evaluation requires some computational effort because standard quadratures (e.g., Gauss-Legendre formulas) cannot be used. Therefore, this choice does not seem very promising.

In conclusion, the next sections discuss how to solve the integration of (2) in the case of linear (affine) curvature and torsion, both in the case when a closed form solution exists, and also when a numerical tool is necessary. The contribution of the present paper is twofold, we provide the first closed form solution that can be applied to a family of curves, and when this is not possible, a simple yet effective geometric integrator based on Lie algebra and Magnus Expansion is provided.

3. The clothoid in 3D

To determine the equation of the clothoid, it is necessary to solve the linear system of ordinary differential equations in (2), with the conditions $\kappa(s) = \kappa' s + \kappa_0$ and $\tau(s) = \tau' s + \tau_0$, for real values of $\kappa', \kappa_0, \tau', \tau_0$. The case of a planar curve ($\tau(s) \equiv 0$) has been presented in [54]. In 3D, the general problem takes the form

$$\boldsymbol{y}'(s) = \boldsymbol{A}(s)\boldsymbol{y}(s), \qquad \boldsymbol{y}(0) = \boldsymbol{y}_0, \tag{4}$$

with matrix $\boldsymbol{A}(s)$ given by

$$\boldsymbol{A}(s) = \begin{bmatrix} 0 & \kappa(s) & 0 \\ -\kappa(s) & 0 & \tau(s) \\ 0 & -\tau(s) & 0 \end{bmatrix};$$

finally, $\boldsymbol{y} = [\boldsymbol{t}^T, \boldsymbol{n}^T, \boldsymbol{b}^T]^T \in \mathbb{R}^9$ is the vector of the coordinates of the intrinsic frame and $\boldsymbol{y}_0$ is the initial point.

Remark 3. The matrix $\boldsymbol{A}(s)$ is skew-symmetric, and the space of such matrices forms the Lie Algebra of the orthogonal group. When discussing existence and convergence, the eigenvalues of $\boldsymbol{A}^T\boldsymbol{A}$ are required, they are zero and $Q(s) := \kappa(s)^2 + \tau(s)^2$.

With the standard notation $\boldsymbol{y}'(s) = \boldsymbol{A}(s)\boldsymbol{y}(s)$, the problem is written as a linear system of ODEs with non constant coefficients, also known as linear time variant system (LTV system), originating at $\boldsymbol{y}(0) = \boldsymbol{y}_0$. The existence and uniqueness of the solution are ensured by the Lipschitz continuity of $\boldsymbol{A}(s)$ and fundamental results of differential equations, e.g. the Cauchy-Lipschitz theorem. For scalar equations, the solution can be obtained by the classic variation of constants formula; for higher dimensions, that formula, intended with matrix exponentials instead of the usual, is valid in particular cases only, that is, if and only if a condition based on the commutator is satisfied. A first property of the LTV system (4) is its stability, as it is proved in the next proposition.

Proposition 1 (Stability)**.** *The autonomous linear time variant system (4) is stable.*

Proof. The quadratic function $V(\boldsymbol{y}) = ||\boldsymbol{y}||^2$ (with $||\cdot||$ is the Euclidean norm) is a Lyapunov function, since V is defined everywhere, $V(\boldsymbol{0}) = 0$ and $V(\boldsymbol{y}) > 0$ for all $\boldsymbol{y} \neq \boldsymbol{0}$. Now let $\boldsymbol{y}(s)$ be a solution of (4), then, taking the derivative with respect to s:

$$V'(\boldsymbol{y}(s)) = \boldsymbol{y}'^T\boldsymbol{y} + \boldsymbol{y}^T\boldsymbol{y}' = \boldsymbol{y}^T(\boldsymbol{A}^T + \boldsymbol{A})\boldsymbol{y} = 0,$$

since $\boldsymbol{A}^T + \boldsymbol{A} = \boldsymbol{0}$, being $\boldsymbol{A}$ skew-symmetric. Thus, the LTV system is stable. □

The initial value problem (4) is best studied in a slightly extended framework, in the Lie Groups, where we follow the works of [50,52]. In order to do this, we consider the *matrix* linear differential equation

$$\boldsymbol{Y}'(s) = \boldsymbol{A}(s)\boldsymbol{Y}(s), \qquad \boldsymbol{Y}(0) = \boldsymbol{Y}_0. \tag{5}$$

In this setting, $\boldsymbol{Y}_0 \in G$, where G is a Lie group, $\boldsymbol{A} : \mathbb{R}^+ \to \mathfrak{g}$ is a Lipschitz continuous matrix and $\mathfrak{g}$ is the Lie algebra of G. Here, a Lie group G is a finite dimensional differentiable real manifold, where the product of elements and its inversion are smooth. The corresponding Lie algebra $\mathfrak{g}$ is the tangent space of G, i.e., the set of all possible values that can take $\gamma'(0)$,

where $\gamma(t) \in G$ is a smooth curve, and $\gamma(0) = I_d$, the identity of G. Precisely, for the problem at hand, $\boldsymbol{Y}$ belongs to the orthogonal group O and the matrix $\boldsymbol{A}$ to the (special) orthogonal Lie algebra $\mathfrak{so}$.

The most relevant fact with respect to our problem, is that the Lie algebra is closed under the second operation, the Lie bracket or commutator: let g_1 and g_2 be elements of $\mathfrak{g}$, then $[g_1, g_2] := g_1 g_2 - g_2 g_1 \in \mathfrak{g}$ and it also satisfies the Jacobi identity. This is important because any combination of operations remains in the group, which means that properties of the initial point are preserved by any numerical method that acts on the Lie structure.

Wilhelm Magnus, in his seminal paper [55], proposed to write the solution of (5) as an exponential of a series of matrices, called the Magnus Expansion (ME). Other possible choices for similar series expansions are the Dyson series, the Fer method, the Symmetric Fer method, the Cayley method and the Wilcox expansion. In [50,52] it is shown how to construct the above methods starting from the ME, hence, in this work, we focus only on the ME. The solution proposed by Magnus is to write the solution of (5) as

$$\boldsymbol{Y}(s) = e^{\boldsymbol{\Omega}(s)} \cdot \boldsymbol{Y}_0, \qquad \boldsymbol{\Omega}(s) = \sum_{i=1}^{\infty} \boldsymbol{\Omega}_i(s). \tag{6}$$

The first two terms of the Magnus expansion are easily produced, [52],

$$\boldsymbol{\Omega}_1(s) = \int_0^s \boldsymbol{A}(s_1)\, \mathrm{d}s_1,$$
$$\boldsymbol{\Omega}_2(s) = \frac{1}{2}\int_0^s [\boldsymbol{\Omega}_1(s_1), \boldsymbol{A}(s_1)]\, \mathrm{d}s_1.$$

Higher order terms can be computed via recursion relations, but cannot be employed naively because they involve an increasing number of nested commutators and multidimensional integrals (efficient practical numerical schemes are discussed later).

The bracket in $\boldsymbol{\Omega}_2$ corresponds exactly to the commutator condition stated next, and is contained in all other terms $\boldsymbol{\Omega}_i$; this shows how the ME reduces to the standard formula of variation of constants whenever the condition is satisfied, as $\boldsymbol{\Omega}_i = 0$ for $i \geq 2$, so that $\boldsymbol{Y}(s) = \exp(\boldsymbol{\Omega}_1(s))\boldsymbol{Y}_0$.

Definition 1 (Commutator)**.** Let $\boldsymbol{\Omega}_1(s) = \int_0^s A(\sigma)\, \mathrm{d}\sigma$ be the integral of the coefficient matrix $\boldsymbol{A}$ of the system $\boldsymbol{y}'(s) = \boldsymbol{A}(s)\boldsymbol{y}(s)$. The commutator condition is satisfied if $[\boldsymbol{\Omega}_1, \boldsymbol{A}] = \boldsymbol{\Omega}_1\boldsymbol{A} - \boldsymbol{A}\boldsymbol{\Omega}_1 = \boldsymbol{0}$.

A sufficient test (but not necessary, [55]) for the above commutator condition, is that for any pair of different values of the independent variable, say s_1 and s_2, the equality $\boldsymbol{A}(s_1)\boldsymbol{A}(s_2) = \boldsymbol{A}(s_2)\boldsymbol{A}(s_1)$ holds. For the problem at hand, the commutator condition is given in the next proposition.

Proposition 2. *The commutator condition for $\boldsymbol{y}'(s) = \boldsymbol{A}(s)\boldsymbol{y}(s)$ is equivalent to $m := \kappa'\tau_0 - \tau'\kappa_0 = 0$.*

Proof. The integral of the curvature and the torsion are $\frac{1}{2}\kappa' s^2 + \kappa_0 s$ and $\frac{1}{2}\tau' s^2 + \tau_0 s$, respectively. Thus, matrix $\boldsymbol{\Omega}_1$ reads

$$\boldsymbol{\Omega}_1 = \begin{bmatrix} 0 & \kappa' s^2/2 + \kappa_0 s & 0 \\ -\kappa' s^2/2 - \kappa_0 s & 0 & \tau' s^2/2 + \tau_0 s \\ 0 & -\tau' s^2/2 - \tau_0 s & 0 \end{bmatrix}. \tag{7}$$

The Lie bracket $[\boldsymbol{\Omega}_1, \boldsymbol{A}]$ is a simple matrix operation and reads

$$[\boldsymbol{\Omega}_1, \boldsymbol{A}] = \frac{ms^2}{2}\begin{bmatrix} 0 & 0 & -1 \\ 0 & 0 & 0 \\ 1 & 0 & 0 \end{bmatrix},$$

with $m = \kappa'\tau_0 - \tau'\kappa_0$. Thus, the commutator condition is satisfied if and only if $m = 0$. □

In general, however, the commutator condition is not satisfied, and this requires to consider, at least formally, the complete series of the ME, which poses the additional problems of existence and convergence of the series. The answers to these fundamental questions are given in the following theorem, that is adapted for the problem at hand from the theorem of Magnus and its refinements.

Theorem 4 (Magnus Expansion)**.** *The differential Eq. (5) has a solution of the form (6), where the exponent lies in the Lie algebra $\mathfrak{so}$ and is a continuous differentiable function of $\boldsymbol{A}(s)$. Finally $\boldsymbol{\Omega}$ can be computed with the Magnus expansion (6) for $0 \leq s \leq S$, with $S = \max\left\{s \geq 0\ s.t.\ \int_0^s Q(\sigma)\, \mathrm{d}\sigma \leq \pi\right\}$, where $Q(s) = \kappa(s)^2 + \tau(s)^2$, as defined in Remark 3.*

Proof. The theorem is adapted from [52]. The interval $S = \max\left\{s \geq 0\ s.t.\ \int_0^s ||\boldsymbol{A}(\sigma)||_2\, \mathrm{d}\sigma \leq \pi\right\}$, gives the convergence of the series, which can be simplified, thanks to Remark 3, e.g., $||\boldsymbol{A}(\sigma)||_2 = Q(\sigma)$, which is the spectral radius of $\boldsymbol{A}^T\boldsymbol{A}$ ($||\cdot||_2$ is the usual matrix 2-norm). □

The theorem is useful to recognise that the ME is valid only locally, hence in view of designing a numerical method, the overall integration interval must be divided into steps, so that the ME converges in each sub interval. A limitation of

these geometric integrators that preserve the Lie structure is that they require to evaluate the terms $\boldsymbol{\Omega}_i$, which in turn need the computation of a large number of nested commutators and their integration. Then, after the truncated series has been determined, it must be exponentiated, which is also a difficult task [56]. These methods become attractive if the above issues could be solved and if the integration step can be made bigger than the one of usual integrators, e.g. Euler or Runge-Kutta. For the problem at hand, all these issues can be solved in closed form and they are discussed in the following section, then; in Section 5, closed form solutions are presented for the particular cases in which the commutator condition holds.

4. Geometric integrators for the general clothoid case

In this section we discuss how to overcome the issues presented at the end of the previous section and illustrate a geometric Magnus integrator that gives accurate results at the price of a light computational cost compared to other methods.

The first issue to address is to write the terms $\boldsymbol{\Omega}_i$, reducing the otherwise enormous number of nested commutators. This problem has been solved by Iserles and Nørsett in [50] by means of binary trees, and in [52] exploiting the time symmetry of the ME. For instance, the fourth order Magnus Geometric integrator (MG4) presented in [52] requires only two of them. The next step is to evaluate the involved integrals, which for our problem is not difficult do to since the functions appearing in $\boldsymbol{A}$ are polynomials, so they can be easily integrated in closed form. Indeed, the MG4 presented in [50,52] uses Gauss-Legendre integration, which is exact for polynomials of low degree and requires only two matrix evaluations and two commutators, hence it is also possible to skip the explicit integration step, as the two results will coincide. The third step is the computation of the matrix exponential in (6), which is, in general, the costliest operation of the integration step. Common methods include scaling and squaring with Pad approximations, the Chebyshev method, computation in Krylov spaces; there are various splitting methods and also a number of other "dubious" methods, [56]. In our case, the particular structure of $\boldsymbol{A}(s)$ and of the truncated series for $\boldsymbol{\Omega}$ makes it possible to write the truncated expansion $e^{\boldsymbol{\Omega}}$ in closed form. Therefore, we have recast each integration-exponentiation step of the numerical method MG4 into a simple matrix-vector product and two matrix evaluations.

The complexity of the MG4 integrator will be reduced in Section 4.1 by exploiting some closed form expressions that the present problem offers, but it can be barely extended to higher methods. The two main difficulties are the presence of lots of nested commutators and the final matrix exponential. Higher order methods can be designed using a commutator-free approach [57,58], which is discussed and specialised for clothoids in Section 4.2, where the method CF4GL is described.

Before describing the two methods, we point out that problem (4) (respectively problem (5)) gives the solution of the Frenet-Serret frame, but the curve is obtained with a successive integration of the tangent vector. Although it is possible to compute $\boldsymbol{t}$ via the ME (6) and then use the obtained points as input to a second integration method that gives the clothoid, we prefer to insert this integration step directly in (4) (respectively problem (5)), by stacking an identity block below matrix $\boldsymbol{A}(s)$. Precisely, we define matrix $\boldsymbol{B} \in \mathbb{R}^{12\times 12}$ as follows:

$$\boldsymbol{B}(s) = \begin{bmatrix} 0 & \kappa(s) & 0 & 0 \\ -\kappa(s) & 0 & \tau(s) & 0 \\ 0 & -\tau(s) & 0 & 0 \\ 1 & 0 & 0 & 0 \end{bmatrix} \otimes \boldsymbol{I}_3.$$

Clearly, we also extend the vector $\boldsymbol{y} \in \mathbb{R}^9$ to $\boldsymbol{x} \in \mathbb{R}^{12}$ by defining $\boldsymbol{x} = [\boldsymbol{t}^T, \boldsymbol{n}^T, \boldsymbol{b}^T, x(s), y(s), z(s)]^T$, where the last components are the desired parametric equations of the clothoid curve. Although this disrupts the Lie algebra $\mathfrak{so}$ as it is enlarged to the general linear group $\mathfrak{gl}$, in practice, the orthonormality of the Frenet-Serret frame is preserved, as it discussed in the following section of numerical tests.

4.1. Truncated ME with order 4 Gaussian points - MG4

The method to solve $\boldsymbol{x}'(s) = \boldsymbol{B}(s)\boldsymbol{x}(s)$ is to employ the truncated Magnus Expansion (6). A method of order 4 is obtained considering the first two terms of the ME; in general, a method of order $2p$, for $p \geq 2$, requires terms up to Ω_{2p-2}, [52]. Then, since the Magnus series only converges locally (Theorem 4), it is necessary to split the integration interval $[0, S]$ into n subintervals of amplitude $h = L/n$ so that the abscissa is $s_i = ih$, for $i = 0, 1, 2, \ldots, n$. The generic step is given by $\boldsymbol{x}_{i+1} = e^{\boldsymbol{E}_i}\boldsymbol{x}_i$, where $\boldsymbol{E}_i := \boldsymbol{\Omega}_1 + \boldsymbol{\Omega}_2$, is the truncated ME evaluated at s_i, which requires two function evaluations (a_1, a_2), one commutator $([a_2, a_1])$ and the computation of the exponential of $\boldsymbol{E}_i$, see [52] or [50]. To avoid the integration step, the two points Gauss-Legendre quadrature is applied [59]:

$$\boldsymbol{E}_i = \frac{h}{2}(a_1 + a_2) + \frac{\sqrt{3}h^2}{12}[a_2, a_1], \qquad a_1 := \boldsymbol{B}\big(s_i + \big(1/2 - \sqrt{3}/6\big)h\big), \qquad a_2 := \boldsymbol{B}\big(s_i + \big(1/2 + \sqrt{3}/6\big)h\big), \tag{8}$$

This computation can be reduced to a matrix-vector product at each step by exploiting the particular form of the matrices involved and by carrying out analytic steps of linear algebra. Matrix $\boldsymbol{E}_i$ has the simple form

$$\boldsymbol{E}_i = \begin{bmatrix} 0 & \ell_1 & \ell_3 & 0 \\ -\ell_1 & 0 & \ell_2 & 0 \\ -\ell_3 & -\ell_2 & 0 & 0 \\ h & \ell_4 & 0 & 0 \end{bmatrix},$$

where the coefficients ℓ_j for $j = 1, \dots, 4$ are:

$$\ell_1 := \kappa' h^2 (i + 1/2) + \kappa_0 h, \qquad \ell_2 := \tau' h^2 (i + 1/2) + \tau_0 h, \qquad \ell_3 := m h^3/12, \qquad \ell_4 := -\kappa' h^3/12. \tag{9}$$

To compute the matrix exponential of $\boldsymbol{E}_i$, the method of exact eigen decomposition is used here. The matrix cannot be diagonalized, as the geometric and algebraic multiplicity of the eigenvalues are not the same, thus the Jordan decomposition must be used: $\boldsymbol{QJQ}^{-1} = \boldsymbol{E}_i$, where

$$\boldsymbol{J} = \begin{bmatrix} 0 & 1 & 0 & 0 \\ 0 & 0 & 0 & 0 \\ 0 & 0 & \boldsymbol{i}\lambda & 0 \\ 0 & 0 & 0 & -\boldsymbol{i}\lambda \end{bmatrix}, \qquad \lambda = \sqrt{\ell_1^2 + \ell_2^2 + \ell_3^2}, \tag{10}$$

$\boldsymbol{Q}$ and $e^{\boldsymbol{E}_i}$ are given in terms of the auxiliary quantities

$$\lambda\zeta_1 := \ell_1^2 h + \ell_3(\ell_{24} + \ell_3 h), \lambda\zeta_2 := \ell_1\ell_{14} + \ell_2(\ell_{24} + \ell_3 h),$$

$$\lambda\zeta_3 := -\ell_1(\ell_2 h - \ell_{34}),$$

where $\ell_{ij} := \ell_i \ell_j$ for $i, j = 1, \dots, 4$, e.g., $\ell_{12} = \ell_1\ell_2$. The complex valued matrix $\boldsymbol{Q}$ is readily obtained, and is:

$$\boldsymbol{Q} = \frac{1}{2\lambda^2} \begin{bmatrix} 0 & 2\ell_2^2 & \ell_1^2 + \ell_3^2 & \ell_1^2 + \ell_3^2 \\ 0 & -2\ell_{23} & \ell_{23} + \boldsymbol{i}\lambda\ell_1 & \ell_{23} - \boldsymbol{i}\lambda\ell_1 \\ 0 & 2\ell_{12} & -\ell_{12} + \boldsymbol{i}\lambda\ell_3 & -\ell_{12} - \boldsymbol{i}\lambda\ell_3 \\ q_{41} & q_{42} & q_{43} & q_{44} \end{bmatrix},$$

with the coefficients q_{4j}, for $j = 1, \dots, 4$ given by

$$q_{41} = 2\ell_2(\ell_2 h - \ell_{34}), \qquad q_{42} = -2\ell_{14}, \qquad q_{43} = \ell_{14} - \frac{\boldsymbol{i}}{\lambda}(h(\ell_1^2 + \ell_3^2) + \ell_2\ell_{34}), \qquad q_{44} = \boldsymbol{i}\zeta_1 + \ell_{14}.$$

The matrix exponential is then equal to $e^{\boldsymbol{E}_i} = 1/\lambda^2 \boldsymbol{C}$, where:

$$\boldsymbol{C} = \begin{bmatrix} (\ell_1^2 + \ell_3^2)c_\lambda + \ell_2^2 & \lambda\ell_1 s_\lambda - \ell_{23}\tilde{c}_\lambda & \lambda\ell_3 s_\lambda + \ell_{12}\tilde{c}_\lambda & 0 \\ -\lambda\ell_1 s_\lambda - \ell_{23}\tilde{c}_\lambda & (\ell_1^2 + \ell_2^2)c_\lambda + \ell_3^2 & \lambda\ell_2 s_\lambda - \ell_{13}\tilde{c}_\lambda & 0 \\ -\lambda\ell_3 s_\lambda + \ell_{12}\tilde{c}_\lambda & -\lambda\ell_2 s_\lambda - \ell_{13}\tilde{c}_\lambda & (\ell_2^2 + \ell_3^2)c_\lambda + \ell_1^2 & 0 \\ c_{41} & c_{42} & c_{43} & \lambda^2 \end{bmatrix}, \tag{11}$$

$$\begin{aligned} c_{41} &= \zeta_1 s_\lambda - \ell_{14}\tilde{c}_\lambda + \ell_2(\ell_2 h - \ell_{34}), \\ c_{42} &= \zeta_2 s_\lambda + h\ell_1\tilde{c}_\lambda - (\ell_{23} h - \ell_3\ell_{34}), \\ c_{43} &= \zeta_3 s_\lambda + (\ell_{24} + \ell_3\, h)\tilde{c}_\lambda + (\ell_{12} h - \ell_1\ell_{34}), \end{aligned}$$

and, finally, $s_\lambda := \sin\lambda, \quad c_\lambda := \cos\lambda, \quad \tilde{c}_\lambda := 1 - \cos\lambda$.

This analytic construction gives a boosts in the numerical performance, as it requires, at each step s_i, only the evaluations of a_1 and a_2 and a matrix-vector multiplication $e^{\boldsymbol{E}_i}\boldsymbol{x}_i$. This saves many time consuming 12×12 matrix routines at each step, namely the nested commutators to compute matrix $\boldsymbol{E}_i$ and the matrix exponential that can be evaluated exactly with the Jordan factorization of $\boldsymbol{E}_i$, which requires a matrix inversion. Loosing the opportunity of explicitly developing the numerical method reducing its computational cost to a matrix-vector product for each step, it is possible to design similar geometric methods of higher order and also implement variable stepsize strategies for error control, but this theme is out of the scope of the present study.

Algorithm 1 MG4. Input: n discretisation points, L length, clothoid parameters.

$h \leftarrow L/n$;
$Y_0 \leftarrow y_0$;
for $i = 0, 1, 2, \dots, n$ **do**
  Evaluate C and λ using (11), (10), (9)
  $Y_{i+1} = \frac{1}{\lambda^2}\, C \otimes I_3 \cdot Y_i$; that is, $e^{E_i} = e^{Omega_1 + Omega_2}$
end for
Output: the solution $Y = [t^T, n^T, b^T, x, y, z]$

4.2. Commutator-Free integrators of order 4 with Gauss-Legendre points - CF4GL

As discussed in the previous section, the Magnus Expansion is a powerful tool for solving linear differential equations, especially when they have an underlying Lie group structure. However, from a practical point of view, the ME is rather involved, [57]: a fourth order method requires 7 nested commutators, which can be reduced to two. These numbers quickly grow, e.g., for a sixth order method 22 commutators needs to be analysed and reduced to 7, and for a method of order eight they are 70 (reducible to 22). The commutator-free approach is effective because it preserves the Lie group structure of the equation but it avoids the use of commutators. It approximates the solution of the problem with an expansion of type $e^{\boldsymbol{B}_1}e^{\boldsymbol{B}_2}\cdots e^{\boldsymbol{B}_k}$, where each $\boldsymbol{B}_i=\sum_m g_{i,m}\boldsymbol{B}(s_m)$, that is, a finite linear combination of $\boldsymbol{B}(s)$ at different nodes.

The Commutator-Free method of order 4 with Gauss-Legendre points (CF4GL) is defined by a pair of exponentials $e^{\boldsymbol{B}_1}e^{\boldsymbol{B}_2}$:

$$e^{\boldsymbol{B}_1}e^{\boldsymbol{B}_2}=e^{h(\alpha a_1+\beta a_2)}\cdot e^{h(\beta a_1+\alpha a_2)},\qquad \alpha:=\frac{3-2\sqrt{3}}{12},\qquad \beta:=\frac{3+2\sqrt{3}}{12},$$

where h is the integration step, a_1 and a_2 are the evaluations of the matrix $\boldsymbol{B}(s)$ at the Gauss-Legendre points (defined in (8)), α and β are the coefficients $g_{i,m}$ of the linear combination of $\boldsymbol{B}(s)$ used for the quadrature. Explicit closed form expressions for $e^{\boldsymbol{B}_1}$ and $e^{\boldsymbol{B}_2}$ are now derived, so that the integration step reduces to a matrix product, without the need of computing expensive matrix exponential, thus keeping the overall computational effort reduced. The matrices $\boldsymbol{B}_1$ and $\boldsymbol{B}_2$ can be written as

$$\boldsymbol{B}_1=h\begin{bmatrix}0&c_1&0&0\\-c_1&0&c_2&0\\0&-c_2&0&0\\\alpha+\beta&0&0&0\end{bmatrix},\qquad \boldsymbol{B}_2=h\begin{bmatrix}0&d_1&0&0\\-d_1&0&d_2&0\\0&-d_2&0&0\\\alpha+\beta&0&0&0\end{bmatrix},$$

with entries ($\nu_1=s_i+\left(1/2-\sqrt{3}/6\right)h$ and $\nu_2=s_i+\left(1/2+\sqrt{3}/6\right)h$ are the Gauss-Legendre points):

$$\begin{array}{lcllcl}c_1&=&\alpha(h\kappa'\nu_1+\kappa_0)+\beta(h\kappa'\nu_2+\kappa_0) & d_1&=&\beta(h\kappa'\nu_1+\kappa_0)+\alpha(h\kappa'\nu_2+\kappa_0)\\ c_2&=&\alpha(h\tau'\nu_1+\tau_0)+\beta(h\tau'\nu_2+\tau_0) & d_2&=&\beta(h\tau'\nu_1+\tau_0)+\alpha(h\tau'\nu_2+\tau_0)\\ c^2&=&c_1^2+c_2^2 & d^2&=&d_1^2+d_2^2.\end{array}\tag{12}$$

To find the exponetial of $\boldsymbol{B}_1$ and $\boldsymbol{B}_2$ the Jordan decomposition is used, which yields $\boldsymbol{B}_1=\boldsymbol{Q}_1\boldsymbol{J}_1\boldsymbol{Q}_1^{-1}$ and $\boldsymbol{B}_2=\boldsymbol{Q}_2\boldsymbol{J}_2\boldsymbol{Q}_2^{-1}$, with

$$\boldsymbol{J}_1=\begin{bmatrix}0&1&0&0\\0&0&0&0\\0&0&\boldsymbol{i}ch&0\\0&0&0&-\boldsymbol{i}ch\end{bmatrix},\qquad \boldsymbol{Q}_1=\frac{1}{2c^3}\begin{bmatrix}0&2c\,c_2^2&c\,c_1^2&c\,c_1^2\\0&0&\boldsymbol{i}c^2c_1&-\boldsymbol{i}c^2c_1\\0&2c\,c_1c_2&-c\,c_1c_2&-c\,c_1c_2\\2h(\alpha+\beta)c\,c_2^2&0&-\boldsymbol{i}(\alpha+\beta)c_1^2&\boldsymbol{i}(\alpha+\beta)c_1^2\end{bmatrix};$$

and matrices $\boldsymbol{J}_2$ and $\boldsymbol{Q}_2$ relative to $\boldsymbol{B}_2$ have the same structure of $\boldsymbol{J}_1$ and $\boldsymbol{Q}_1$ but with the corresponding coefficients "d" instead of "c".

The final step is to take the exponential of the Jordan form and simplify the terms, which gives:

$$e^{\boldsymbol{B}_1}=\frac{1}{c^3}\begin{bmatrix}c\left(c_1^2\cos(hc)+c_2^2\right)&c^2\,c_1\sin(hc)&c\,c_1c_2(1-\cos(hc))&0\\-c^2\,c_1\sin(hc)&c^3\cos(hc)&c^2\,c_2\sin(hc)&0\\c\,c_1c_2(1-\cos(hc))&-c^2\,c_2\sin(hc)&c\left(c_2^2\cos(hc)+c_1^2\right)&0\\(\alpha+\beta)\left(hc\,c_2^2+c_1^2\sin(hc)\right)&(\alpha+\beta)c\,c_1(1-\cos(hc))&(\alpha+\beta)c_1c_2(hc-\sin(hc))&c^3\end{bmatrix},\tag{13}$$

and $e^{\boldsymbol{B}_2}$ has the same structure of $e^{\boldsymbol{B}_1}$ with coefficients "d" instead of "c".

The final algorithm can be summarised as:

Algorithm 2 CF4GL. Input: n discretisation points, L length, clothoid parameters.

$h\leftarrow L/n$;
$Y_0\leftarrow y_0$;
for $i=0,1,2,\ldots,n$ **do**
  Evaluate e^{B_1} and e^{B_2} using (13), (12)
  $Y_{i+1}=(e^{B_1}\cdot e^{B_2})\otimes I_3\cdot Y_i$;
end for
Output: the solution $Y=[t^T,n^T,b^T,x,y,z]$

The design of commutator-free integrators of order higher than 4 requires some care, since the coefficients of the quadrature need to satisfy a positivity condition to be stable, [60].

5. Clothoids that satisfy the commutator condition

The exposition of the previous section is general and can be applied to any choice of curvature and torsion coefficients. Indeed, if the commutator condition $m = 0$ is satisfied, we can derive a closed form solution that involves the standard Fresnel integrals only. This happens in two cases of interest, when $\kappa(s) = \kappa' s$ and $\tau(s) = \tau' s$, which we call the *canonical* clothoid (curvature and torsion are linear); the second case is when curvature and torsion are affine, which we call *general* clothoid (still satisfying $m = 0$, however).

5.1. Canonical clothoid: $\kappa(s) = \kappa' s$ and $\tau(s) = \tau' s$

This case represents the classic curve, often referred to as Euler spiral, in which the curvature and the torsion are both linear, but not affine with the arc length, whereas the affine case is usually called clothoid. Assuming that the commutator condition is satisfied, it is possible to express the solution in terms of the matrix exponential and to obtain closed form solutions applying the matrix version of the variation of constants formula.

Proposition 3 (Eigen decomposition of. $\boldsymbol{\Omega}_1$) *The matrix $\boldsymbol{\Lambda}$ of the eigenvalues and the matrix $\boldsymbol{H}$ of the eigenvectors of $\boldsymbol{\Omega}_1$ in (7) for $\kappa(s) = \kappa' s$ and $\tau(s) = \tau' s$ are*

$$\boldsymbol{\Lambda} = \frac{s^2}{2}\begin{bmatrix} 0 & 0 & 0 \\ 0 & \boldsymbol{i}\sqrt{\Delta} & 0 \\ 0 & 0 & -\boldsymbol{i}\sqrt{\Delta} \end{bmatrix} \otimes \boldsymbol{I}_3, \qquad \boldsymbol{H} = \begin{bmatrix} \tau' & -\kappa' & -\kappa' \\ 0 & -\boldsymbol{i}\sqrt{\Delta} & \boldsymbol{i}\sqrt{\Delta} \\ \kappa' & \tau' & \tau' \end{bmatrix} \otimes \boldsymbol{I}_3,$$

where $\Delta := \kappa'^2 + \tau'^2$ and $\boldsymbol{\Omega}_1 = \boldsymbol{H}\boldsymbol{\Lambda}\boldsymbol{H}^{-1}$.

Proof. It is a classic exercise of linear algebra. □

Proposition 4 (Exponential of. $\boldsymbol{\Omega}_1$) *The matrix exponential of $\boldsymbol{\Omega}_1$ for $\kappa(s) = \kappa' s$ and $\tau(s) = \tau' s$ is given by*

$$e^{\boldsymbol{\Omega}_1} = \frac{1}{\Delta}\begin{bmatrix} \kappa'^2 C(s) + \tau'^2 & \sqrt{\Delta}\kappa' S(s) & \kappa'\tau'(1 - C(s)) \\ -\sqrt{\Delta}\kappa' S(s) & \Delta C(s) & \sqrt{\Delta}\tau' S(s) \\ \kappa'\tau'(1 - C(s)) & -\sqrt{\Delta}\tau' S(s) & \tau'^2 C(s) + \kappa'^2 \end{bmatrix},$$

where $C(s) = \cos(\sqrt{\Delta}s^2/2)$ and $S(s) = \sin(\sqrt{\Delta}s^2/2)$.

Proof. From the eigen decomposition of $\boldsymbol{\Omega}_1$ of Proposition 3, it follows that $\boldsymbol{H}^{-1}$ is

$$\boldsymbol{H}^{-1} = \frac{1}{\Delta}\begin{bmatrix} \tau' & 0 & \kappa' \\ -\kappa'/2 & \boldsymbol{i}\sqrt{\Delta}/2 & \tau'/2 \\ -\kappa'/2 & -\boldsymbol{i}\sqrt{\Delta}/2 & \tau'/2 \end{bmatrix}.$$

The matrix exponential of $\boldsymbol{\Omega}_1$ is constructed using the relation $\boldsymbol{\Omega}_1 = \boldsymbol{H}\boldsymbol{\Lambda}\boldsymbol{H}^{-1}$ together with its Taylor's series

$$e^{\boldsymbol{\Omega}_1} = \sum_{k=0}^{\infty} \frac{\boldsymbol{\Omega}_1^k}{k!} = \sum_{k=0}^{\infty} \frac{\boldsymbol{H}\boldsymbol{\Lambda}^k\boldsymbol{H}^{-1}}{k!} = \boldsymbol{H}e^{\boldsymbol{\Lambda}}\boldsymbol{H}^{-1}.$$

In fact, $\boldsymbol{\Omega}_1^k = \boldsymbol{H}\boldsymbol{\Lambda}\boldsymbol{H}^{-1}\cdots\boldsymbol{H}\boldsymbol{\Lambda}\boldsymbol{H}^{-1} = \boldsymbol{H}\boldsymbol{\Lambda}^k\boldsymbol{H}^{-1}$, the exponential of a diagonal matrix is the exponential of the diagonal elements, i.e. the eigenvalues. The exponential $e^{\boldsymbol{\Lambda}}$ is obtained combining the exponentials with Euler's relation. □

The explicit relation for the Frenet-Serret frame is obtained multiplying $e^{\boldsymbol{\Omega}_1}$ with the vector of the initial conditions, $\boldsymbol{y}_0 = [\boldsymbol{t}_0, \boldsymbol{n}_0, \boldsymbol{b}_0]^T$. In conclusion, the following equation expresses the vectors of the Frenet frame: $e^{\boldsymbol{\Omega}_1} \cdot \boldsymbol{y}_0 = [\boldsymbol{t}(s), \boldsymbol{n}(s), \boldsymbol{b}(s)]^T$, where,

$$\begin{aligned} \boldsymbol{t}(s) &= \tfrac{1}{\Delta}\left(\left(\kappa'^2 C(s) + \tau'^2\right)\boldsymbol{t}_0 + \sqrt{\Delta}\kappa' S(s)\boldsymbol{n}_0 + \kappa'\tau'(1 - C(s))\boldsymbol{b}_0\right) \\ \boldsymbol{n}(s) &= \tfrac{1}{\sqrt{\Delta}}\left(-\kappa' S(s)\boldsymbol{t}_0 + \sqrt{\Delta}C(s)\boldsymbol{n}_0 + \tau' S(s)\boldsymbol{b}_0\right) \\ \boldsymbol{b}(s) &= \tfrac{1}{\Delta}\left(\kappa'\tau'(1 - C(s))\boldsymbol{t}_0 - \sqrt{\Delta}\tau' S(s)\boldsymbol{n}_0 + \left(\tau'^2 C(s) + \kappa'^2\right)\boldsymbol{b}_0\right). \end{aligned} \tag{14}$$

From (14) it is possible to give the explicit equations of a 3D canonical clothoid in terms of the Fresnel integrals.

Theorem 5 (3D canonical clothoid)**.** *The arc length parametric equations of a 3D canonical clothoid γ, starting at the origin with the initial Frenet-Serret frame $[\boldsymbol{t}_0^T, \boldsymbol{n}_0^T, \boldsymbol{b}_0^T]^T$, with curvature $\kappa(s) = \kappa' s$ and torsion $\tau(s) = \tau' s$, are given by*

$$\gamma(s) = \frac{\left(\kappa'^2 \mathcal{C}(s) + \tau'^2 s\right)\boldsymbol{t}_0 + \sqrt{\Delta}\kappa' \mathcal{S}(s)\boldsymbol{n}_0 + \kappa'\tau'(s - \mathcal{C}(s))\boldsymbol{b}_0}{\Delta}, \tag{15}$$

where $\Delta = \kappa'^2 + \tau'^2$ and the Fresnel integrals $\mathcal{C}(s)$, $\mathcal{S}(s)$ are

$$\mathcal{C}(s) = \int_0^s \cos\left(\frac{\sqrt{\Delta}\xi^2}{2}\right) \mathrm{d}\xi, \qquad \mathcal{S}(s) = \int_0^s \sin\left(\frac{\sqrt{\Delta}\xi^2}{2}\right) \mathrm{d}\xi.$$

Proof. To prove that the given space curve is parametrised by arc length, the condition $||\gamma'|| = 1$ must hold. Since $||\gamma'|| = ||\boldsymbol{t}||$, from (14) it is obtained

$$||\boldsymbol{t}||^2 = \frac{1}{\Delta^2}\left(\left(\kappa'^2 C(s) + \tau'^2\right)^2 + \Delta\kappa'^2 S(s)^2 + \kappa'^2\tau'^2(C(s)-1)^2\right)$$

because $\boldsymbol{t}_0$, $\boldsymbol{n}_0$, $\boldsymbol{b}_0$ are orthonormal vectors. Applying the trigonometric identity $C(s)^2 + S(s)^2 = 1$ yields

$$||\boldsymbol{t}||^2 = \frac{1}{\Delta^2}\left(\kappa'^4 + 2\kappa'^2\tau'^2 + \tau'^4\right) = \frac{(\kappa'^2+\tau'^2)^2}{\Delta^2} = 1.$$

The linearity of the curvature $\kappa(s) = ||\boldsymbol{t}'|| = |\kappa' s|$ must hold:

$$\begin{aligned}||\boldsymbol{t}'||^2 &= \frac{1}{\Delta^2}\left(\Delta\kappa'^4 s^2 S(s)^2 + \Delta^2\kappa'^2 s^2 C(s) + \Delta\kappa'^2\tau'^2 s^2 S(s)^2\right)\\ &= \frac{1}{\Delta^2}\left(S(s)^2 s^2\kappa'^2(\kappa'^2\Delta + \tau'^2\Delta - \Delta^2) + \Delta^2\kappa'^2 s^2\right)\\ &= \frac{1}{\Delta^2}\left(\Delta^2\kappa'^2 s^2\right) = \kappa'^2 s^2.\end{aligned}$$

Since $\tau(s) = -\boldsymbol{b}^{\cdot}\cdot\boldsymbol{n} = \tau^{\cdot}s$, the derivative of $\boldsymbol{b}$ is

$$\boldsymbol{b}^{\cdot} = \frac{1}{\sqrt{\Delta}}\left(\kappa^{\cdot}\tau^{\cdot} s S(s)\boldsymbol{t}_0 - \sqrt{\Delta}\tau^{\cdot} s C(s)\boldsymbol{n}_0 - \tau^{\cdot 2}\, s S(s)\boldsymbol{b}_0\right),$$

so that the scalar product $\boldsymbol{b}'\cdot\boldsymbol{n}$ yields

$$-\boldsymbol{b}^{\cdot}\cdot\boldsymbol{n} = \frac{1}{\Delta}\left(\tau^{\cdot 3}\, s S(s)^2 + \Delta\tau^{\cdot} s C(s)^2 + \kappa^{\cdot 2}\tau^{\cdot} s S(s)^2\right) = \frac{1}{\Delta}\left(\left(\left(\kappa^{\cdot 2}+\tau^{\cdot 2}\right)S(s)^2 + \Delta C(s)^2\right)\tau^{\cdot} s\right) = \tau^{\cdot} s.$$

The curve discussed in the theorem naturally blends to a standard planar clothoid if the torsion vanishes and maintains all the analytic properties such as arc length and linear curvature. □

Remark 6. Interestingly enough, the evaluation of a point on a 3D canonical clothoid (15) has approximately the same computational cost of a planar clothoid, as it requires only two Fresnel integrals and some elementary operations.

5.2. General clothoid: $\kappa(s) = \kappa' s + \kappa_0$ and $\tau(s) = \tau' s + \tau_0$

The general case with affine curvature and torsion that respect the commutator condition $m = 0$ can be obtained repeating the computations of the previous section for the canonical clothoid, this time with affine curvature $\kappa(s) = \kappa' s + \kappa_0$ and torsion $\tau(s) = \tau' s + \tau_0$. The proofs are omitted since they are similar to the proofs of the equivalent results shown for the canonical case, there are only a few more terms. Only the steps needed to build the solution are reported, indeed the outline is the same.

Proposition 5 (Eigen decomposition of. $\boldsymbol{\Omega}_1$) *The matrices $\boldsymbol{\Lambda}$ and $\boldsymbol{H}$ of the eigenvalues and eigenvectors of $\boldsymbol{\Omega}_1$ are:*

$$\boldsymbol{\Lambda} = \frac{s}{2}\begin{bmatrix}0 & 0 & 0\\ 0 & \boldsymbol{i}\sqrt{Q(s)} & 0\\ 0 & 0 & -\boldsymbol{i}\sqrt{Q(s)}\end{bmatrix}, \qquad \boldsymbol{H} = \begin{bmatrix}T(s) & -K(s) & -K(s)\\ 0 & -\boldsymbol{i}\sqrt{Q(s)} & \boldsymbol{i}\sqrt{Q(s)}\\ K(s) & T(s) & T(s)\end{bmatrix},$$

where $Q(s) := K(s)^2 + T(s)^2$, $K(s) = \kappa(s) + \kappa_0$, $T(s) = \tau(s) + \tau_0$ and $\boldsymbol{\Omega}_1 = \boldsymbol{H}\boldsymbol{\Lambda}\boldsymbol{H}^{-1}$.

Proposition 6 (Exponential of. $\boldsymbol{\Omega}_1$) *The matrix exponential of $\boldsymbol{\Omega}_1$ for curvature $\kappa(s) = \kappa' s + \kappa_0$ and torsion $\tau(s) = \tau' s + \tau_0$ is given by (dropping the explicit dependence of s):*

$$e^{\boldsymbol{\Omega}_1} = \frac{1}{Q}\begin{bmatrix}K^2 C_Q + T^2 & \sqrt{Q}KS_Q & KT(1-C_Q)\\ -\sqrt{Q}KS_Q & QC_Q & \sqrt{Q}TS_Q\\ KT(1-C_Q) & -\sqrt{Q}TS_Q & T^2C_Q + K^2\end{bmatrix},$$

with $Q(s) = K(s)^2 + T(s)^2$, $K(s) = \kappa(s) + \kappa_0$, $T(s) = \tau(s) + \tau_0$ and $C_Q(s) = \cos\left(\sqrt{Q(s)}s/2\right)$, $S_Q(s) = \sin\left(\sqrt{Q(s)}s/2\right)$.

The explicit relation for the Frenet-Serret frame is obtained multiplying $e^{\boldsymbol{\Omega}_1}$ by the vector $\boldsymbol{y}_0$ of the initial conditions:

$$\begin{aligned}\boldsymbol{t}(s) &= \tfrac{1}{Q}\left(\left(K^2C_Q + T^2\right)\boldsymbol{t}_0 + \sqrt{Q}KS_Q\boldsymbol{n}_0 + KT(1-C_Q)\boldsymbol{b}_0\right),\\ \boldsymbol{n}(s) &= \tfrac{1}{\sqrt{Q}}(-KS_Q\boldsymbol{t}_0 + C_Q\boldsymbol{n}_0 + TS_Q\boldsymbol{b}_0),\\ \boldsymbol{b}(s) &= \tfrac{1}{Q}\left(KT(1-C_Q)\boldsymbol{t}_0 + \sqrt{Q}TS_Q\boldsymbol{n}_0 + \left(T^2C_Q + K^2\right)\boldsymbol{b}_0\right).\end{aligned}$$

From the above solution, it is possible to give the equations of a 3D clothoid by integrating the tangent vector $\boldsymbol{t}$.

Lemma 7 (3D clothoid)**.** *The arc length parametric equations of a 3D clothoid γ, starting with the configuration $[\boldsymbol{t}_0^T, \boldsymbol{n}_0^T, \boldsymbol{b}_0^T]^T$, with curvature $\kappa(s) = \kappa' s + \kappa_0$ and torsion $\tau(s) = \tau' s + \tau_0$, whose coefficients satisfy the commutator condition $m = \kappa'\tau_0 - \tau'\kappa_0 = 0$, are given by*

$$\gamma(s) = \int_0^s \frac{1}{Q(s)} \left(\left(K(s)^2 C_Q(s) + T(s)^2\right)\boldsymbol{t}_0 + \sqrt{Q(s)}K(s)S_Q(s)\boldsymbol{n}_0 + K(s)T(s)(1 - C_Q(s))\boldsymbol{b}_0 \right) \mathrm{d}s,$$

with $Q(s)$, $K(s)$ and the other values defined in Proposition 6.

The above equations do not have the inexpensive computational cost of Theorem 5, indeed they involve non standard special functions as Fresnel integrals with rational parameters, thus they are not well suited for high performance computing.

In the spirit of Euler's practice of giving more than one proof of his results, there is a second and more elegant way to obtain the solution given in Lemma 7, which relies on a geometrical observation. A general clothoid has two inflection points at s_κ and s_τ (see Fig. 2): when either the curvature or the torsion are zero. This happens, respectively, if $s = s_\kappa = -\kappa_0/\kappa'$ or $s = s_\tau = -\tau_0/\tau'$. A clothoid that satisfies the commutator condition has $s_\kappa = s_\tau$, since $m = \kappa'\tau_0 - \tau'\kappa_0 = 0$, that is $\kappa_0/\kappa' = \tau_0/\tau'$, because it is assumed that $\kappa' \neq 0$, $\tau' \neq 0$ (otherwise the curve is not a proper 3D clothoid). This means that the general clothoid that satisfies the commutator condition can be obtained from a canonical clothoid (that has both curvature and torsion inflection at the origin) by an appropriate shift of the curvilinear abscissa s and by a rigid motion. To better describe this reduction to canonical case, it is convenient to introduce some notation. Let $\mathcal{C}$ be the canonical clothoid described in Theorem 5, $\mathcal{G}$ the general clothoid that satisfies the commutator condition given in Lemma 7 and $\mathcal{N}$ one numeric routine to handle a general clothoid discussed in Section 4. It is convenient to approach the problem from an algorithmic point of view: suppose that each curve is evaluated at a certain parameter s and it returns the corresponding point in space $\boldsymbol{p}_s$, the associated Frenet-Serret frame $\boldsymbol{t}_s$, $\boldsymbol{n}_s$ and $\boldsymbol{b}_s$. A superscript is introduced to identify the different curves:

$$\begin{aligned}
\left[\boldsymbol{p}_s^{\mathcal{C}}, \boldsymbol{t}_s^{\mathcal{C}}, \boldsymbol{n}_s^{\mathcal{C}}, \boldsymbol{b}_s^{\mathcal{C}}\right] &= \mathcal{C}(s; \boldsymbol{p}_0, \boldsymbol{t}_0, \boldsymbol{n}_0, \boldsymbol{b}_0, \kappa', \tau'),\\
\left[\boldsymbol{p}_s^{\mathcal{G}}, \boldsymbol{t}_s^{\mathcal{G}}, \boldsymbol{n}_s^{\mathcal{G}}, \boldsymbol{b}_s^{\mathcal{G}}\right] &= \mathcal{G}(s; \boldsymbol{p}_0, \boldsymbol{t}_0, \boldsymbol{n}_0, \boldsymbol{b}_0, \kappa', \tau', \kappa_0, \tau_0),\\
\left[\boldsymbol{p}_s^{\mathcal{N}}, \boldsymbol{t}_s^{\mathcal{N}}, \boldsymbol{n}_s^{\mathcal{N}}, \boldsymbol{b}_s^{\mathcal{N}}\right] &= \mathcal{N}(s; \boldsymbol{p}_0, \boldsymbol{t}_0, \boldsymbol{n}_0, \boldsymbol{b}_0, \kappa', \tau', \kappa_0, \tau_0),
\end{aligned}$$

where $\boldsymbol{p}_0$ is the base point, $[\boldsymbol{t}_0^T, \boldsymbol{n}_0^T, \boldsymbol{b}_0^T]^T$ is the initial Frenet-Serret frame, κ' and τ' are the coefficients of the derivative of curvature and torsion, κ_0 and τ_0 are the initial curvature and torsion. Clearly, if $\kappa_0 = \tau_0 = 0$, we have the equality $\mathcal{C} = \mathcal{G} = \mathcal{N}$; also, if the commutator condition is satisfied, i.e. $m = 0$, then $\mathcal{G} = \mathcal{N}$. It is now discussed how to write $\mathcal{G}$ in terms of $\mathcal{C}$, thus avoiding the integrals of Lemma 7.

Theorem 8 (Reduction to canonical)**.** *Let a general clothoid $\mathcal{G}$ satisfy the commutator condition of Lemma 7 origin at $\boldsymbol{p}_0^{\mathcal{G}}$ with initial Frenet-Serret frame $[\boldsymbol{t}_0^{\mathcal{G}}, \boldsymbol{n}_0^{\mathcal{G}}, \boldsymbol{b}_0^{\mathcal{G}}]$, initial curvature κ_0, initial torsion τ_0, curvature derivative κ', torsion derivative τ'. Then, $\mathcal{G}$ can be evaluated in terms of the canonical clothoid $\mathcal{C}$ by means of the relation*

$$\mathcal{G}\left(s; \boldsymbol{p}_0^{\mathcal{G}}, \boldsymbol{t}_0^{\mathcal{G}}, \boldsymbol{n}_0^{\mathcal{G}}, \boldsymbol{b}_0^{\mathcal{G}}, \kappa', \tau', \kappa_0, \tau_0\right) = \mathcal{C}\left(s - \bar{s}; \boldsymbol{p}_0^{\mathcal{G}} - \boldsymbol{p}_T^{\mathcal{C}}, \boldsymbol{t}_0^{\mathcal{C}}, \boldsymbol{n}_0^{\mathcal{C}}, \boldsymbol{b}_0^{\mathcal{C}}, \kappa', \tau'\right),$$

where the new parameters are computed using (16) and (17) and $\bar{s} = -\kappa_0/\kappa' = -\tau_0/\tau'$ is the abscissa of the inflection point.

Proof. To evaluate the clothoid $\mathcal{G}$ in terms of $\mathcal{C}$ we start from its general configuration $\mathcal{G}(s; \boldsymbol{p}_0^{\mathcal{G}}, \boldsymbol{t}_0^{\mathcal{G}}, \boldsymbol{n}_0^{\mathcal{G}}, \boldsymbol{b}_0^{\mathcal{G}}, \kappa', \tau', \kappa_0, \tau_0)$. Since the commutator condition holds, the inflection point is at the curvilinear abscissa $\bar{s}$. The configuration at $\bar{s}$ represents the initial condition for the canonical clothoid $\mathcal{C}$, and is obtained going backwards:

$$\left[\boldsymbol{p}_0^{\mathcal{C}}, \boldsymbol{t}_0^{\mathcal{C}}, \boldsymbol{n}_0^{\mathcal{C}}, \boldsymbol{b}_0^{\mathcal{C}}\right] = \mathcal{C}\left(-\bar{s}; \boldsymbol{0}, \boldsymbol{t}_0^{\mathcal{G}}, \boldsymbol{n}_0^{\mathcal{G}}, \boldsymbol{b}_0^{\mathcal{G}}, -\kappa', -\tau'\right). \tag{16}$$

Finally, the base point of the canonical clothoid $\mathcal{C}$ (that starts at the origin) must be shifted to match the initial point of application of $\mathcal{G}$: this is the space travelled by the curve $\mathcal{C}$ with the new parameters obtained in (16), i.e.:

$$\left[\boldsymbol{p}_T^{\mathcal{C}}, \cdot, \cdot, \cdot\right] = \mathcal{C}\left(-\bar{s}; \boldsymbol{0}, \boldsymbol{t}_0^{\mathcal{C}}, \boldsymbol{n}_0^{\mathcal{C}}, \boldsymbol{b}_0^{\mathcal{C}}, \kappa', \tau'\right). \tag{17}$$

The new initial point and the shift of the curvilinear abscissa by $\bar{s}$ yield the result. □

Remark 9. Theorem 8 is a fundamental result that enables to take advantage of the closed form equation in terms of the standard Fresnel integrals of the canonical clothoid given in Theorem 5. This prompts an efficient and practical use of these curves in the applications and avoids the need for the demanding numerical integration of the equations of Lemma 7, or the numerical method based on the Magnus Expansion. The only limitation is the requirement of satisfying the commutator condition, or, in other words, to have a unique and coincident inflection point for both curvature and torsion.

6. Numerical tests and comparisons

In this section we compare our specialised Magnus integrators with some of the usual integrators, namely the implicit Euler scheme, the explicit Runge-Kutta scheme of order 4, the diagonally implicit three stage Runge-Kutta of order

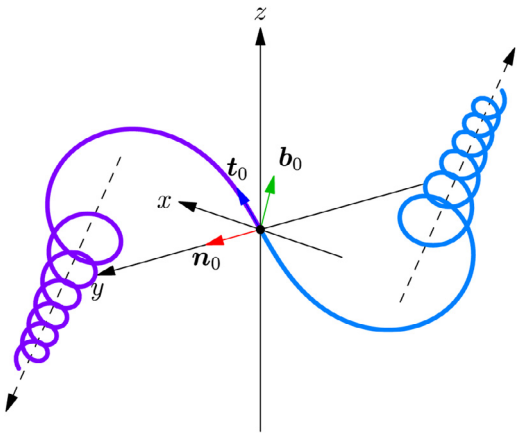

Fig. 1. Canonical clothoid of data $\kappa_0 = \tau_0 = 0$ and $\kappa' = -\tau' = 1/2$.

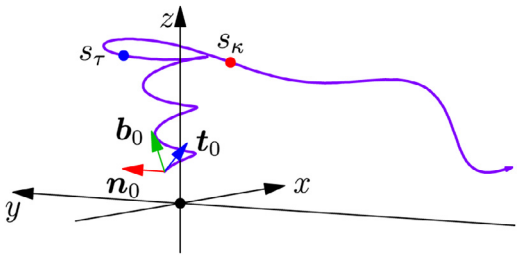

Fig. 2. A general space clothoid of data $\boldsymbol{p}_0 = [1, 1, 1]^T$, $\boldsymbol{t}_0 = [\sqrt{3}/2, 0, 1/2]^T$, $\boldsymbol{n}_0 = [0, 1, 0]^T$, $\boldsymbol{b}_0 = [-1/2, 0, \sqrt{3}/2]^T$, $\kappa' = 1/6$, $\tau' = 1/10$, $\kappa_0 = -5/2$, $\tau_0 = -1$, displayed for $s \in [0, 20]$. The inflection point of the curvature (red dot) is at $s_\kappa = 15$, the inflection of the torsion (blue dot) is at $s_\tau = 10$. In this case $m = 1/12 \neq 0$. (For interpretation of the references to colour in this figure legend, the reader is referred to the web version of this article.)

4 [61] (S361) and the Maple implementation of the implicit Runge-Kutta of order 4 with variable step size. They are sorted in increasing quality. We compare the results in terms of accuracy with respect to the exact solution given by Theorem 5. We also compare the norm of the tangent, normal and binormal vectors of the Frenet-Serret frame, as well as their orthonormality.

The implicit Euler method has step $\boldsymbol{x}_{i+1} = \boldsymbol{x}_i + hf(s_{i+1}, \boldsymbol{x}_{i+1})$ with $f(s, \boldsymbol{x}) := \boldsymbol{B}(s)\boldsymbol{x}$ and can be made explicit by solving the sparse linear system with coefficient matrix $\boldsymbol{S} := \boldsymbol{I} - h\boldsymbol{B}$ at each step. We note in passing, that $\boldsymbol{I} - h\boldsymbol{A}$ is always non singular, being $\boldsymbol{A}$ skew-symmetric, thus allowing an explicit step of the implicit Euler method. Among the explicit Runge-Kutta methods of order 4, we choose the classic scheme given by the tableau ([61] S322)

0				
1/2	1/2			
1/2	0	1/2		
1	0	0	1	
	1/6	1/3	1/3	1/6

For the three stage diagonally implicit Runge-Kutta scheme of order 4, the Butcher tableau [61] (S361) is

x	x		
1/2	$1/2 - x$	x	
$1 - x$	$2x$	$1 - 4x$	x
	$\frac{1}{6(1-2x)^2}$	$\frac{3(1-2x)^2-1}{3(1-2x)^2}$	$\frac{1}{6(1-2x)^2}$

where x is one of the roots of $x^3 - 3/2x^2 + x/2 - 1/24$. The root $x^\star$ that gives the best results is

$$x^\star = \frac{\sqrt{3}}{12}\left(\cos\frac{7\pi}{18} + \cos\frac{5\pi}{18}\right) + \frac{1}{4}\left(\cos\frac{\pi}{9} + \cos\frac{2\pi}{9}\right) + \frac{1}{2}.$$

We tested the algorithms on a 3D clothoid of parameters $\kappa' = 1/2$, $\tau' = -1/2$, $\kappa_0 = 0$ and $\tau_0 = 0$. These values clearly satisfy the commutator condition $m = 0$ so that Theorem 5 can be applied and the numerical results can be compared with

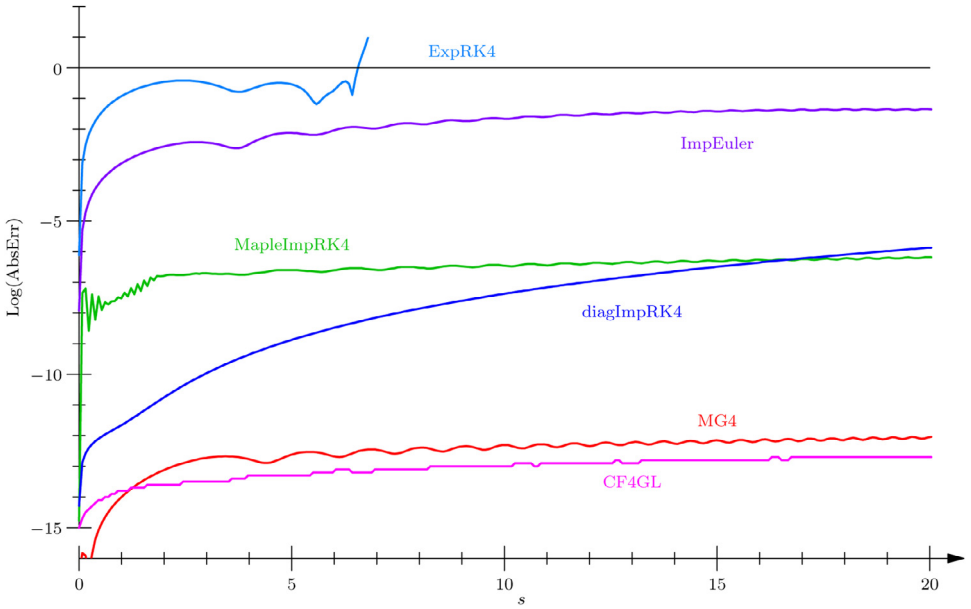

Fig. 3. Logarithm of the absolute error for the considered methods over a grid with $n = 6539$. The geometric integrators perform better than the standard, CF4GL is slightly better than MG4.

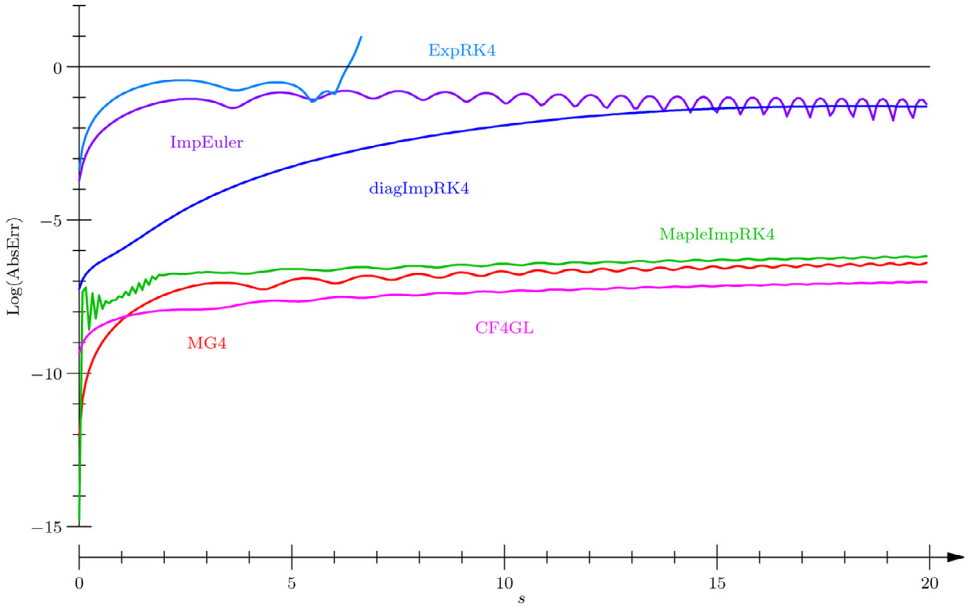

Fig. 4. Logarithm of the absolute error for the considered methods over a grid with $n = 256$, where the MG4 and CF4GL methods have the same accuracy of Maple's implicit RK4 with error control and variable stepsize.

the exact solution. The initial conditions are given by $\boldsymbol{t}_0 = [\sqrt{3}/2, 0, 1/2]^T$, $\boldsymbol{n}_0 = [0, 1, 0]^T$, $\boldsymbol{b}_0 = [-1/2, 0, \sqrt{3}/2]^T$, the base point is the origin, see Fig. 1. The integration interval is $s \in [0, L]$ with $L = 20$.

In the first test, we compare the performance of the various methods in terms of accuracy and of number of function evaluations. In the case of the Maple implementation of the implicit RK method of order 4 with error control, the default error tolerance is set to 10^{-6}, which is achieved with $n = 6539$ function evaluations. For the other methods, it is possible to tune the integration step only (respectively the number of steps), thus we compare the methods over a grid of $n = 6539$ points. The results can be graphically evaluated in Fig. 3.

Since the problem is stiff, the explicit RK4 method has the worst performance; the implicit Euler method, despite its simple form, yields a reasonably good result and also a comforting stable behaviour; the Maple implementation of the implicit RK4 is of course flat below the threshold 10^{-6}; the diagonally implicit RK4 has good performance, but is not very

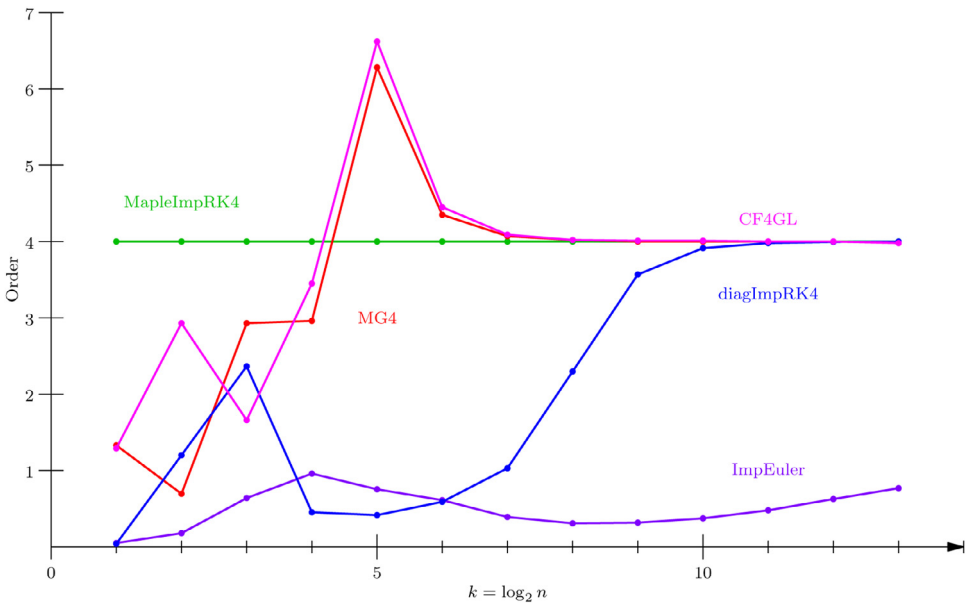

Fig. 5. Graph of the estimation of the order for the considered methods, evaluating $\log_2(\mathrm{err}_{2n}/\mathrm{err}_n)$ for meshes of size $n = 2^k$ and $k = 1, \ldots, 14$. The geometric integrators MG4 and CF4GL have the same behaviour.

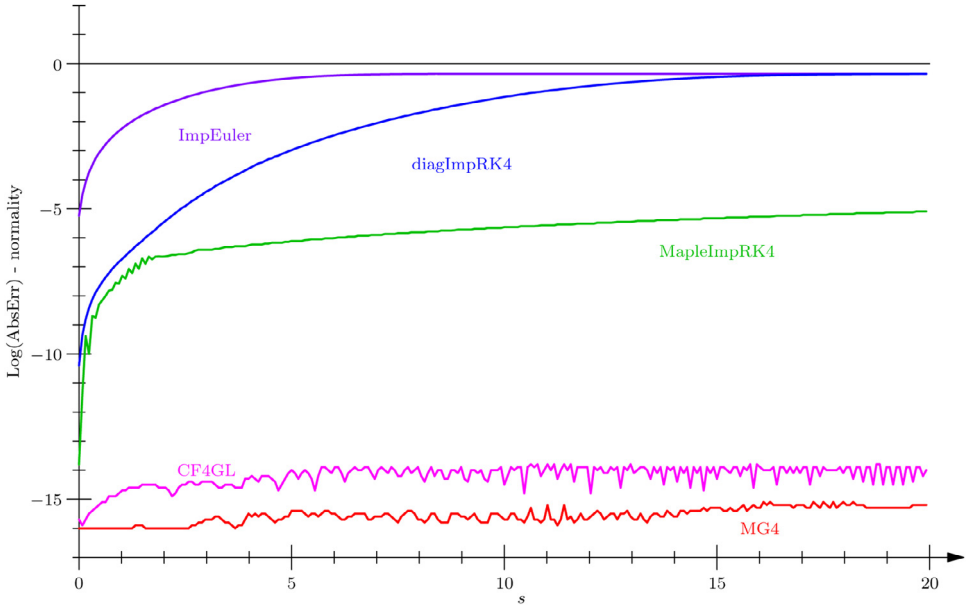

Fig. 6. Logarithm of the absolute error of the norm of the Frenet-Serret frame, $||\boldsymbol{t}|| + ||\boldsymbol{n}|| + ||\boldsymbol{b}|| - 3$ with a mesh with $n = 256$. Here the MG4 performs better than the CF4GL in preserving the group structure of the solution, indeed both are very close to machine precision.

stable as the integration domain increases. Finally, the present methods MG4 and CF4GL show a flat behaviour around 10^{-13} and are therefore competitive also from the computational point of view because the time consuming operations (like the commutators, the integration of the multi-dimensional integrals and matrix exponentiation, to be repeated at each step) are calculated analytically and just a matrix-vector multiplication is required at each step.

Another comparison has been done with respect to the error threshold: we look at the minimum number of integration steps (function evaluations) for the MG4 method to satisfy an overall error below 10^{-6}. It turns out this number is around $n = 256$, see Fig. 4. It can be noticed that the comments of the other experiment apply also to this case, where MG4 and CF4GL perform well.

In the second test, we verify the order of the methods, thus we discretise the integration interval $[0, L]$ with grids of $n = 2^k$ points, for $k = 1, \ldots, 14$. The integration step is therefore $h = L/2^k$. Figure 5 confirms the orders and also underlines

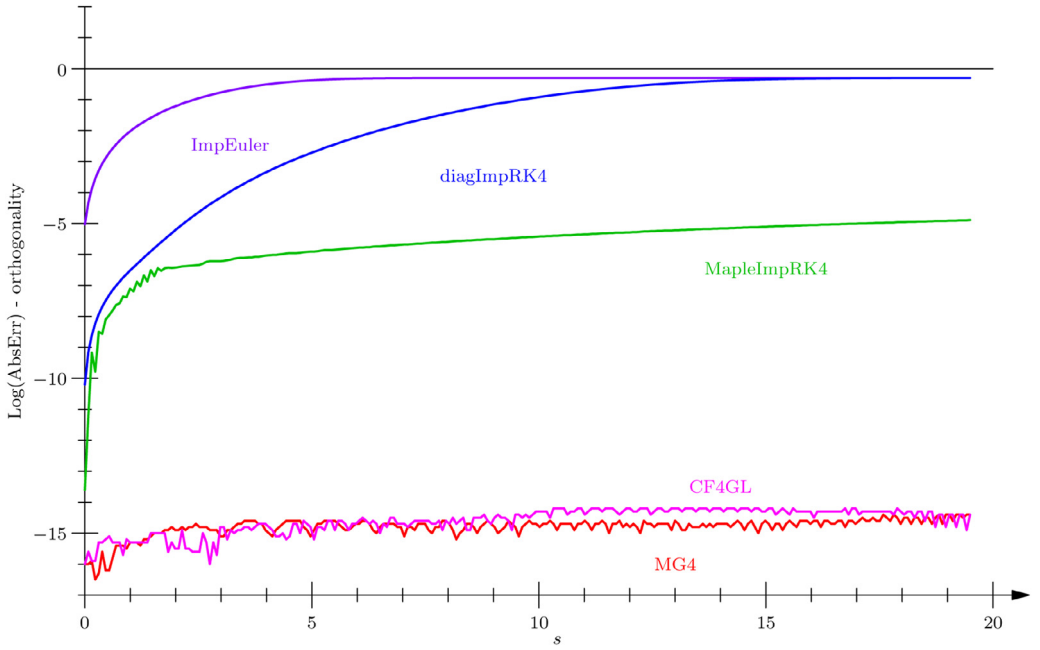

Fig. 7. Logarithm of the absolute error of the orthogonality of the Frenet-Serret frame, $|\boldsymbol{tb}| + |\boldsymbol{tn}| + |\boldsymbol{nb}|$ with a mesh with $n = 256$. The orthogonality of the vectors is well preserved for both MG4 and CF4GL.

the stable behaviour of both MG4 and CF4GL, already for relative coarse meshes with $k = 4$ or 5, whereas the diagonally implicit RK4 needs a finer mesh to reach order 4.

The third experiment checks the orthonormality of the Frenet-Serret frame obtained with the MG4/CF4GL integrators, with the diagonally implicit RK of order 4 and with the Maple implementation of the implicit RK4, over the grid with $n = 256$ points. In Fig. 6 it is displayed the logarithm of the discrepancy from 3 of the sum of the norms of the Frenet-Serret frame, that is $\log_{10}\left|||\boldsymbol{t}|| + ||\boldsymbol{n}|| + ||\boldsymbol{b}|| - 3\right|$. Figure 7 shows the logarithm of the discrepancy from 0 of the sum of the scalar product of the Frenet-Serret frame, that is $\log_{10}(|\boldsymbol{tb}| + |\boldsymbol{tn}| + |\boldsymbol{nb}|)$. From both figures, it is apparent the performance of the presented methods, which are capable of keeping the error at machine precision.

Other results that confirm the effectiveness of MG4 as a general purpose integrator, even without the optimisation steps herein performed, are obtained in [59], where a variety of tests and comparisons are discussed.

7. Conclusions and research perspectives

Thanks to many helpful properties, the clothoid curve is being used in a variety of real-time engineering applications even though it is computationally more demanding than other simpler solutions. So far, the clothoid computation is confined to 2D domains only, which are of obvious interest to model planar motions, typically car-like vehicle trajectories. Nowadays, however, the control of flying vehicle trajectories calls for the development of 3D analytical solutions since an extreme accuracy of computation is required for safety's reasons. The closed form solution (15) of Theorem 5 is derived for the first time in this work and is available when the commutator condition (stated in Proposition 1) is satisfied. When the condition is not satisfied, no closed form exist and two numeric geometric integrators based on the Magnus Expansion and on a Commutator-Free approach are provided. The results are validated with different numerical tests and comparisons with other established numerical methods. This is clearly the first important step towards a practical application of a curve with a number of relevant properties, but there is still much work for the future, in principle all the existing algorithms for clothoid manipulation need to be extended to the 3D case.

References

[1] R. Levien, The Euler Spiral: A Mathematical History, Technical Report UCB/EECS-2008-111, EECS Department, University of California, Berkeley, 2008.
[2] R. Levien, C.H. Séquin, Interpolating splines: which is the fairest of them all? Comput. Aided Des. Appl. 6 (1) (2009) 91–102, doi:10.3722/cadaps.2009.91-102.
[3] D.S. Meek, R.S.D. Thomas, A guided clothoid spline, Comput. Aided Geom. Des. 8 (2) (1991) 163–174, doi:10.1016/0167-8396(91)90042-A.
[4] J. Stoer, Curve fitting with clothoidal splines, J. Res. Nat. Bur. Standards 87 (4) (1982) 317–346, doi:10.6028/jres.087.021.
[5] M. Frego, E. Bertolazzi, F. Biral, D. Fontanelli, L. Palopoli, Semi-analytical minimum time solutions with velocity constraints for trajectory following of vehicles, Automatica 86 (2017) 18–28, doi:10.1016/j.automatica.2017.08.020.
[6] E. Bertolazzi, M. Frego, G^1 fitting with clothoids, Math. Methods Appl. Sci. 38 (5) (2015) 881–897, doi:10.1002/mma.3114.

[7] M. Abramowitz, I. Stegun, Handbook of Mathematical Functions with Formulas, Graphs, and Mathematical Tables, National Bureau of Standards Applied Mathematics Series - 55, U.S. Gove. Printing Office, Washington, D.C., 1964.
[8] A.M. Lekkas, A.R. Dahl, M. Breivik, T.I. Fossen, Continuous-curvature path generation using Fermat's spiral, Model. Identif. Control 34 (4) (2013) 183–198, doi:10.4173/mic.2013.4.3.
[9] E. Bertolazzi, M. Frego, A note on robust biarc computation, Comput. Aided Des. Appl. 16 (5) (2019) 822–835.
[10] J. McCrae, K. Singh, Sketching piecewise clothoid curves, Comput. Graph. 33 (4) (2009) 452–461, doi:10.1016/j.cag.2009.05.006.
[11] I.E. Paromtchik, C. Laugier, Motion generation and control for parking an autonomous vehicle, in: Proc. of IEEE Int. Conference on Robotics and Automation, vol. 4, 1996, pp. 3117–3122.
[12] E. Bakolas, P. Tsiotras, On the generation of nearly optimal, planar paths of bounded curvature and bounded curvature gradient, in: 2009 American Control Conf., 2009, pp. 385–390, doi:10.1109/ACC.2009.5160269.
[13] P.F. Lima, M. Trincavelli, J. Mrtensson, B. Wahlberg, Clothoid-based model predictive control for autonomous driving, in: 2015 European Control Conf. (ECC), 2015, pp. 2983–2990.
[14] J. Funke, J. Christian Gerdes, Simple clothoid lane change trajectories for automated vehicles incorporating friction constraints, J. Dyn. Syst. Meas. Control 138 (2) (2015) 021002, doi:10.1115/1.4032033.
[15] V. Schneider, P. Piprek, S.P. Schatz, T. Baier, C. Drhfer, M. Hochstrasser, A. Gabrys, E. Karlsson, C. Krause, P.J. Lauffs, N.C. Mumm, K. Nrnberger, L. Peter, P. Spiegel, L. Steinert, A. Zollitsch, F. Holzapfel, Online trajectory generation using clothoid segments, in: 2016 14th International Conference on Control, Automation, Robotics and Vision (ICARCV), 2016, pp. 1–6.
[16] M. Frego, P. Bevilacqua, E. Bertolazzi, F. Biral, D. Fontanelli, L. Palopoli, Trajectory planning for car-like vehicles: a modular approach, in: 2016 IEEE 55th Conference on Decision and Control (CDC), 2016, pp. 203–209, doi:10.1109/CDC.2016.7798270.
[17] V.P. Kostov, E.V. Degtiariova-Kostova, The planar motion with bounded derivative of the curvature and its suboptimal paths, Acta Math. Univ. Comenian. (N.S.) 64 (2) (1995) 185–226.
[18] E. Degtiariova-Kostova, V. Kostov, Irregularity of Optimal Trajectories in a Control Problem for a Car-like Robot, Technical Report RR-3411, INRIA, 1998.
[19] D.S. Meek, D.J. Walton, A note on finding clothoids, JCAM 170 (2) (2004) 433–453, doi:10.1016/j.cam.2003.12.047.
[20] D.J. Walton, D.S. Meek, A controlled clothoid spline, Comput. Graph. 29 (3) (2005) 353–363, doi:10.1016/j.cag.2005.03.008.
[21] H.J. Sussmann, The Markov-Dubins problem with angular acceleration control, in: Proceedings of the 36th IEEE Conference on Decision and Control, vol. 3, 1997, pp. 2639–2643, doi:10.1109/CDC.1997.657778.
[22] E. Bertolazzi, M. Frego, On the G^2 hermite interpolation problem with clothoids, J. Comput. Appl. Math. 341 (2018) 99–116, doi:10.1016/j.cam.2018.03.029.
[23] E. Bertolazzi, M. Frego, Interpolating clothoid splines with curvature continuity, Math. Methods Appl. Sci. 41 (4) (2017) 1723–1737, doi:10.1002/mma.4700.
[24] E. Bertolazzi, P. Bevilacqua, M. Frego, Efficient intersection between splines of clothoids, Math Comput. Simul. 176 (2019) 57–72, doi:10.1016/j.matcom.2019.10.001.
[25] E. Bertolazzi, M. Frego, Semianalytical minimum-time solution for the optimal control of a vehicle subject to limited acceleration, Optim. Control Appl. Methods 39 (2) (2018) 774–791, doi:10.1002/oca.2376.
[26] M. Frego, E. Bertolazzi, On the distance between a point and a clothoid curve, in: 2018 European Control Conference (ECC), 2018, pp. 1–6.
[27] M. Frego, E. Bertolazzi, The distance of a point from a clothoid curve, SIAM J. Sci. Comput. 41 (5) (2019) A3326–A3353, doi:10.1137/18M1200439.
[28] E. Bertolazzi, M. Frego, Clothoids: a C++ library with Matlab interface, 2020, https://github.com/ebertolazzi/Clothoids.
[29] E. Bertolazzi, P. Bevilacqua, M. Frego, Clothoids: a C++ library with Matlab interface for the handling of clothoid curves, Rend. Sem. Mat. Univ. Pol. Torino 76 (2) (2018) 47–56.
[30] E. Bertolazzi, P. Bevilacqua, F. Biral, D. Fontanelli, M. Frego, L. Palopoli, Efficient re-planning for robotic cars, in: 2018 European Control Conference (ECC), 2018, pp. 1068–1073, doi:10.23919/ECC.2018.8550215.
[31] J. Ny, E. Feron, E. Frazzoli, On the Dubins traveling salesman problem, IEEE Trans. Autom. Control 57 (1) (2012) 265–270.
[32] M. Frego, P. Bevilacqua, E. Saccon, L. Palopoli, D. Fontanelli, An iterative dynamic programming approach to the multipoint Markov-Dubins problem, IEEE Rob. Autom. Lett. 5 (2) (2020) 2483–2490.
[33] P. Bevilacqua, M. Frego, E. Bertolazzi, D. Fontanelli, L. Palopoli, F. Biral, Path planning maximising human comfort for assistive robots, in: 2016 IEEE Conference on Control Applications (CCA), IEEE, 2016, pp. 1421–1427.
[34] P. Bevilacqua, M. Frego, D. Fontanelli, L. Palopoli, Reactive planning for assistive robots, IEEE Rob. Autom. Lett. 3 (2) (2018) 1276–1283, doi:10.1109/LRA.2018.2795642.
[35] D. Invernizzi, M. Lovera, L. Zaccarian, Dynamic attitude planning for trajectory tracking in thrust-vectoring UAVs, IEEE Trans. Automat. Control 65 (1) (2020) 453–460.
[36] B. Hu, S. Mishra, Time-optimal trajectory generation for landing a quadrotor onto a moving platform, IEEE/ASME Trans. Mechatron. 24 (2) (2019) 585–596.
[37] G. Arechavaleta, J.-P. Laumond, H. Hicheur, A. Berthoz, An optimality principle governing human walking, IEEE Trans. Rob. 24 (1) (2008) 5–14.
[38] G. Arechavaleta, J.-P. Laumond, H. Hicheur, A. Berthoz, On the nonholonomic nature of human locomotion, Auton. Robots 25 (1–2) (2008) 25–35.
[39] T. Luo, H. Chen, G. Kassab, 3D reconstruction of elastin fibres in coronary adventitia, J. Microsc. 265 (1) (2017) 121–131, doi:10.1111/jmi.12470.
[40] E.L. Starostin, R.A. Grant, G. Dougill, G.H. van der Heijden, V.G. Goss, The Euler spiral of rat whiskers, Sci. Adv. 6 (3) (2020) eaax5145.
[41] A.-M. Pendrill, Rollercoaster loop shapes, Phys. Educ. 40 (6) (2005) 517.
[42] Li Guiqing, Li Xianmin, Li Hua, 3D discrete clothoid splines, in: Proc. Computer Graphics International 2001, 2001, pp. 321–324.
[43] M.P. do Carmo, Differential Geometry of Curves and Surfaces, Prentice Hall, 1976.
[44] T.R. Wan, W. Tang, H. Chen, A real-time 3D motion planning and simulation scheme for nonholonomic systems, Simul. Modell. Pract. Theory 19 (1) (2011) 423–439, doi:10.1016/j.simpat.2010.08.002. Modeling and Performance Analysis of Networking and Collaborative Systems
[45] G. Harary, A. Tal, 3D Euler spirals for 3D curve completion, in: Proceedings of the Twenty-Sixth Annual Symposium on Computational Geometry, in: SoCG 10, Association for Computing Machinery, New York, NY, USA, 2010, pp. 393–402, doi:10.1145/1810959.1811025.
[46] D. Ben-Haim, G. Harary, A. Tal, Piecewise 3D Euler spirals, in: Proceedings of the 14th ACM Symposium on Solid and Physical Modeling, in: SPM 10, Association for Computing Machinery, New York, NY, USA, 2010, pp. 201–206, doi:10.1145/1839778.1839810.
[47] G. Harary, A. Tal, Visualizing 3D Euler spirals, in: Proceedings of the Twenty-Sixth Annual Symposium on Computational Geometry, in: SoCG 10, Association for Computing Machinery, New York, NY, USA, 2010, pp. 107–108, doi:10.1145/1810959.1810977.
[48] G. Harary, A. Tal, The natural 3D spiral, Comput. Graph. Forum 30 (2) (2011) 237–246, doi:10.1111/j.1467-8659.2011.01855.x.
[49] R. Casati, F. Bertails-Descoubes, Super space clothoids, ACM Trans. Graph. (TOG) 32 (4) (2013) 1–12.
[50] A. Iserles, S.P. Nrsett, On the solution of linear differential equations in lie groups, Philos. Trans. R. Soc. A 357 (1754) (1999) 983–1019.
[51] A. Iserles, Solving linear ordinary differential equations by exponentials of iterated commutators, Numer. Math. 45 (2) (1984) 183–199.
[52] S. Blanes, F. Casas, J. Oteo, J. Ros, Magnus expansion and some of its applications, Phys. Rep. 470 (5) (2009) 151–238, doi:10.1016/j.physrep.2008.11.001.
[53] Y.J. Kanayama, B.I. Hartman, Smooth local-path planning for autonomous vehicles1, Int. J. Rob. Res. 16 (3) (1997) 263–284, doi:10.1177/027836499701600301.
[54] M. Frego, E. Bertolazzi, On the distance between a point and a clothoid curve, in: 2018 European Control Conference (ECC), 2018, pp. 1–6, doi:10.23919/ECC.2018.8550554.
[55] W. Magnus, On the exponential solution of differential equations for a linear operator, Commun. Pure Appl. Math. 7 (4) (1954) 649–673, doi:10.1002/cpa.3160070404.

[56] C. Moler, C. Van Loan, Nineteen dubious ways to compute the exponential of a matrix, twenty-five years later, SIAM Rev. 45 (1) (2003) 3–49, doi:10.1137/S00361445024180.
[57] A. Alvermann, H. Fehske, High-order commutator-free exponential time-propagation of driven quantum systems, J. Comput. Phys. 230 (15) (2011) 5930–5956, doi:10.1016/j.jcp.2011.04.006.
[58] S. Blanes, F. Casas, M. Thalhammer, High-order commutator-free quasi-magnus exponential integrators for non-autonomouslinear evolution equations, Comput. Phys. Commun. 220 (2017) 243–262, doi:10.1016/j.cpc.2017.07.016.
[59] A. Iserles, A. Marthinsen, S. Nrsett, On the implementation of the method of magnus series for linear differential equations, BIT Numer. Math. 39 (1999) 281–304, doi:10.1023/A:1022393913721.
[60] H. Hofsttter, O. Koch, Non-satisfiability of a positivity condition for commutator-free exponential integrators of order higher than four, Numer. Math. 141 (2019) 681–691, doi:10.1007/s00211-018-1015-x.
[61] J. Butcher, Numerical Methods for Ordinary Differential Equations, Wiley, 2016.